IEEE Access
Multidisciplinary | Rapid Review | Open Access Journal

Received November 16, 2018, accepted November 26, 2018, date of publication November 29, 2018,
date of current version December 27, 2018.

Digital Object Identifier 10.1109/ACCESS.2018.2884029

High-Gain Electrically Large Air-Cavity-Backed Patch Antenna Element and Array

WENFANG PENG[1], WENQUAN CAO[1,2], AND ZUPING QIAN[1]
[1]Department of Communications Engineering, Army Engineering University of PLA, Nanjing 210007, China
[2]State Key Laboratory of Millimeter Waves, Southeast University, Nanjing 210096, China

Corresponding author: Wenquan Cao (cao_wenquan@163.com)

This work was supported by the National Natural Science Foundation of China under Grant 61401506 and Grant 61871399.

ABSTRACT In this paper, single high-gain patch antenna element with electrical large property (ELP) based on TM_{30} mode is presented. Stable field distribution of the TM_{30}-mode is maintained by using one TE_{20}-mode substrate integrated waveguide (SIW) slot-coupling feed structure. Furthermore, air-cavity-backed structure and metal pins are introduced to expand the antenna bandwidth. The ELP element resonates at 22 GHz with simulated −10-dB impedance bandwidth of 6.9% and maximum gain of 14.2 dBi. Then, in order to correct the asymmetrical field distribution in TE_{20}-mode SIW, differential feed technology is introduced in the array design. The feeding network consists of two TE_{10}–TE_{20} mode planar transducers and one anti-phase power divider. The working principle and design procedure of the ELP array are given in detail accordingly. Finally, a 2 × 2 ELP array is optimized and fabricated for verification. The measured results show that the array antenna has −10-dB impedance bandwidth of 9% and maximum gain of 18.9 dBi. Furthermore, it owns merit of excellent radiation performance with high aperture efficiency of about 90%.

INDEX TERMS Array antenna, differential feeding network, electrically large property (ELP), high-aperture efficiency, high-gain, high-order mode, millimeter-wave, mode-transducer.

I. INTRODUCTION

With the rapid development of millimeter wave (MMW) and terahertz (THz) wave systems, high frequency band antennas are attracting more and more research interest recently. They have the advantages of wide bandwidth overcoming the frequency spectrum resource shortage. However, two critical problems could not be ignored in practical applications. The first one is high propagation losses. It is usually solved by enhancing the gain of element and using array technology. Secondly, the fabrication accuracy requirement for MMW and THz devices is too high. Though the high-accuracy technology such as the low temperature co-fired ceramic (LTCC) can solve the problem, the cost is too high. As a result, traditional miniaturization property is no longer the critical requirement for MMW antennas, which is different from the microwave band or other lower bands.

Recently, antennas with electrically large property (ELP) have been used to solve the above problems efficaciously. The best advantage of ELP is their low sensitivity to the fabrication tolerance. Due to the larger aperture of the antenna element, higher gain can be obtained and the feeding network can be designed more flexibly. Some works have been reported on the ELP antennas. On the one hand, dielectric resonator antennas (DRAs) based on high-order mode were designed to achieve ELP [1]. When the DRAs operated in the TE_{115} and TE_{119} mode, the size of the antennas was enlarged by 7 and 14.4 times, respectively. It confirmed that electrically large antennas (ELAs) have lower sensitivity to fabrication tolerance. In [2]–[4], several metallic cavity antennas with ELP were designed, which broke the traditional half-wavelength limit. However, the non-planar structure of both the DRAs and the cavity antennas restricts their practical applications.

On the other hand, some antennas with ELP based on metamaterial structures were designed [5]–[7]. In [5], by dividing the square radiating patch into 4 × 4 elements, the left-handed capacitor was introduced to achieve the composite right-/left-handed transmission-line (CRLH TL) structure. The dispersion curve of the planar structure can be tuned to achieve ELP. Then a theory of electrically large resonant cavity (ELRC) was analyzed in [6]. Based on the theory in [6], one resonant antenna with ELP was designed by loading with I-shaped resonant structures [7]. The resonant frequency increased by 4.6 times comparing with the unloaded one.

However, the design theory is a bit difficult and the meta-based periodical structures are complicated, which will arise problems in practical application and array realization.

Nowadays, high-order mode antennas have been widely explored for gain enhancement [8]–[11], which can also enlarge the electrical size of antennas. However, the bandwidth is too narrow (only about 1%) because of the high quality factor of high-order mode. Furthermore, the excitation condition of the high-order mode is very strict. The TE_{20}-mode substrate integrated waveguide (SIW) double slot feeding structure was first adopted in [12]. However the feeding structure is oversized compared with the antenna working at the fundamental TM_{10} mode, which cause severe side lobe in array application. Thus it is a high light to solve the above problems in this work.

Recently MMW planar array technologies have been reported to obtain high gain property [12]–[16]. The array technology is also necessary in ELA. However, high sidelobes become unavoidable in array design because of the stretched space between the elements. The ELA element with high enough gain can solve the above problem. Furthermore, it can also achieve high gain for array with fewer elements.

In this paper, a novel high-gain patch antenna with ELP based on TM_{30} mode is presented. TE_{20}-mode SIW structure is introduced for feeding. The air-filled cavity back structure is adopted to achieve bandwidth broadening and gain enhancement. By using two TE_{10}-TE_{20} mode transducers and an anti-phase power divider, the differential feeding network can be constituted to feed one 2 × 2 antenna array. The array has stable and symmetrical radiation patterns with good cross-polarization. What's more, high gain property can be obtained by using only four elements, which enhances the aperture and radiation efficiency effectively. The rest of the paper is organized as follows: The high-gain patch antenna element with ELP is presented and analyzed in Section II. Section III analyzes the differential feeding network structure and describes the array performance. The simulated and measured results of the array are presented and discussed in Section IV. Finally conclusion is made in Section V.

II. HIGH-GAIN PATCH ANTENNA ELEMENT WITH ELP

The element antenna resonant on TM_{30} mode is presented in this section. The geometry and operation principle of the element are described in detail. Performance comparisons are made between the proposed one and other structures.

A. THE PATCH ANTENNA RESONANT ON TM_{30} MODE

The high-order mode technology is an effective way to enlarge the electric dimension of the antenna. As is well known, the higher odd-order mode antenna can achieve broadside radiation just like the TM_{10} mode. Nevertheless, the sidelobe level of high-order mode is a severe problem in practical application. In order to decrease the sidelobe level, we try to find the difference between main lobe and sidelobe. The simulated gain and phase patterns on E-plane of the TM_{30} mode are shown in Fig. 1 (a). It can be seen that the antiphase

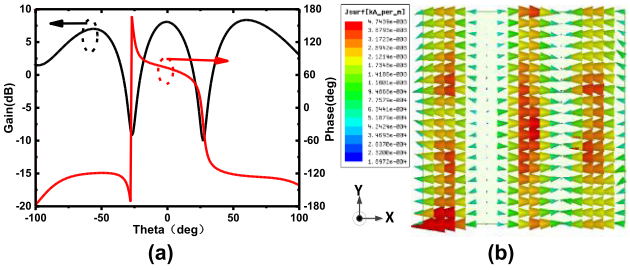

FIGURE 1. The simulated results of the patch antenna resonant on TM_{30} mode. (a) Gain and phase patterns, (b) current distribution.

is excited between main lobe and sidelobe. This difference can be a breakthrough to improve the sidelobe performance of TM_{30} mode. The sidelobe can be lowered or even disappeared by introducing a new radiation field, which is inphase with the main lobe while antiphase with sidelobe. Based on the above analysis, we etched a slot in the center of the patch, which is shown in Fig.2 (a). For the two shorted ends of the slot, the electric field intensity of slot should be modeled as a cosine distribution with respect to the length of slot, which is shown in Fig. 2 (b). The radiation field from the slot is given as [17]

$$E_{\theta S} = -j\frac{L_{S1}W_S k_0 E_0}{4r}e^{-jk_0 r}\sin\phi\frac{\cos X}{(X)^2-(\frac{\pi}{2})^2}\frac{\sin Y}{Y} \quad (1)$$

$$X = \frac{kL_{S1}}{2}sin\theta cos\phi \quad Y = \frac{kW_S}{2}sin\theta sin\phi \quad (2)$$

And the $E_{\theta TM}$ for the patch antenna can be expressed as

$$E_{\theta TM} = j\frac{4k_0 U_{03}}{\lambda_0 r}e^{-jk_0 r}e^{j(\frac{u}{2}+\frac{v}{2})}\sin\frac{u}{2}\cos\frac{v}{2}[\frac{W^2}{u^2}+\frac{W^2}{v^2-(3\pi)^2}] \cdot \sin\theta\sin\phi\cos\phi \quad (3)$$

$$u = k_0 W\sin\theta\cos\phi \quad v = k_0 W\sin\theta\sin\phi \quad (4)$$

Thus the total radiation fields in the upper half space can be written as

$$E_{\theta T} = E_{\theta TS} + E_{\theta TM} \quad (5)$$

Based on the analysis above, it can be found that, since the radiated fields of patch and slot are out of phase, antiphase excitations are required to achieve broadside radiation.

As shown in Fig. 1(b), the current directions at the center and edge of the patch are different. Thus the antiphase excitations can be achieved naturally. The simulated electrical field in Fig. 2 (b) verifies the analysis. The radiation intensity of the slot can be controlled by the length. As shown in Fig.3, the sidelobe level in E-plane decreases or even disappears as the length of the slot increases. However, the beam width in H-plane will be widened, which will cause severe sidelobe in array application. This phenomenon can be explained by the field distribution of patch with one slot in Fig. 2 (b). Due to the slot etched on the patch, the intensity of the field gets weaker near the two edges in H-plane and gets progressively strengthened towards the center of patch, which causes nonuniform

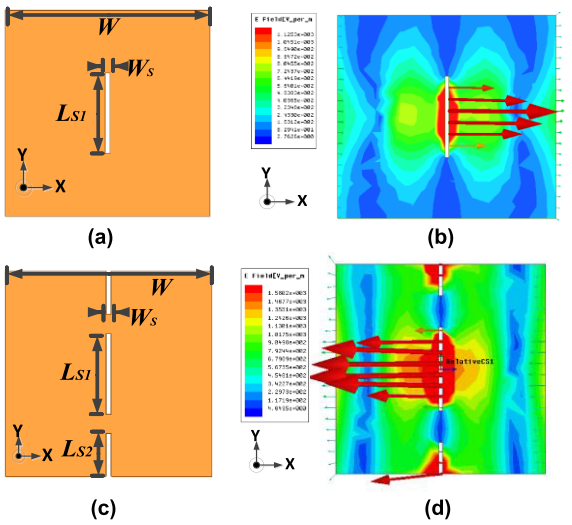

FIGURE 2. Geometries and electric field distribution of two kinds of patches. (a) Geometry of patch with one slot, (b) electric field distribution of the patch with one slot, (c) geometry of patch with three slots, (d) electric field distribution of the patch with three slots.

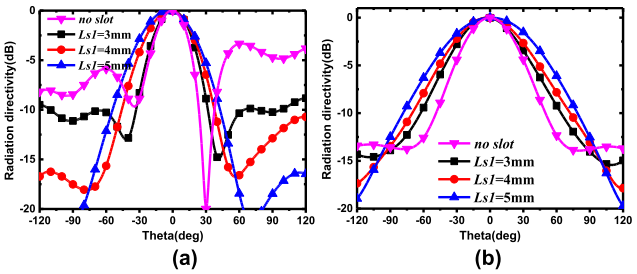

FIGURE 3. The radiation patterns of patch with different slot length of *Ls*1. (a) E-plane, (b) H-plane.

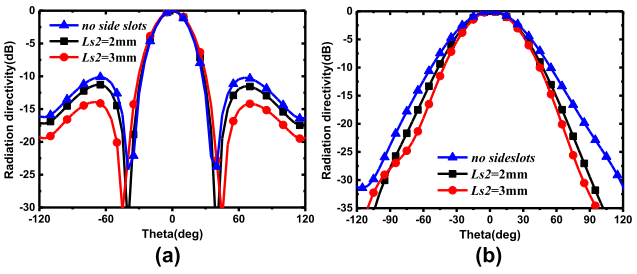

FIGURE 4. The radiation patterns of patch with different slot length of *Ls*2. (a) E-plane, (b) H-plane.

electric field distribution. In order to overcome this problem, two more slots are etched on the edges of the patch which is shown in Fig.2 (d). The two slots make the electric field distribution more uniform. Fig. 4 shows that the beam width in H-plane can be narrowed and the sidelobe level in E-plane can be lowered further by increasing the length of the other two slots *Ls*2.

B. THE CAVITY-BACKED ANTENNA FED BY TE_{20} -MODE SIW

The air-filled cavity backed TM_{30} mode antenna element with ELP is designed. It owns merits of broadband and high

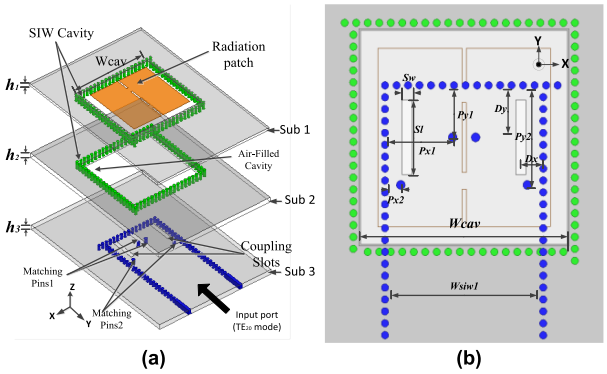

FIGURE 5. The geometry of the antenna element. (a) 3D view, (b) top view.

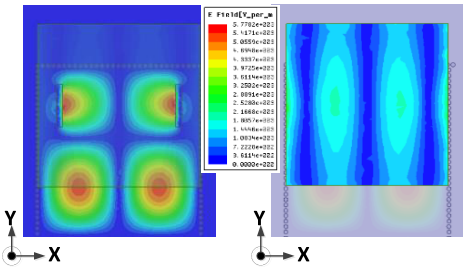

FIGURE 6. The electric field distributions of TE_{20}-mode SIW and TM_{30}-mode patch.

gain performance. The element consists of three dielectric substrate layers, and the geometry is described in Fig. 5

In practical application, stable field distribution of TM_{30} mode plays great impact on the antenna performance within certain bandwidth. In order to excite single TM_{30} mode for the patch antenna element without other low-order modes, the TE_{20}-mode SIW with two coupling slots etched on the surface is adopted as the feeding structure. Fig.6 illustrates the electric field distributions of TE_{20}-mode SIW and the TM_{30}-mode patch. The electric field distributions of SIW and the middle part of the patch are similar with respect to the x-direction. Due to the asymmetry of the TE_{20}-mode field, the slots can generate the cophase excitation by cutting the surface current to maintain the stable field distribution of the TM_{30}-mode patch. The distance between slots and the end of SIW is a quarter of waveguide wavelength. Two pairs of matching pins with radius of 0.25mm, which are symmetrical with the centerline of the TE_{20}-mode SIW, are adopted to add a new resonant point and achieve broadband impedance matching. The matching pins are located at the edges of each subsection of TE_{20} mode, so the pins have little effect on the operation mode.

Due to the strong resonance of the high-order mode, the quality factor is so high that the bandwidth is limited. In order to solve this problem, air-filled cavity backed structure is introduced to reduce the quality factor. Fig.5 shows that the air-filled structure is embedded in Sub.2, and the radiating patch is printed on Sub.1. The cavity is constituted by two SIW structures in Sub 1 and Sub 2. In addition, antenna

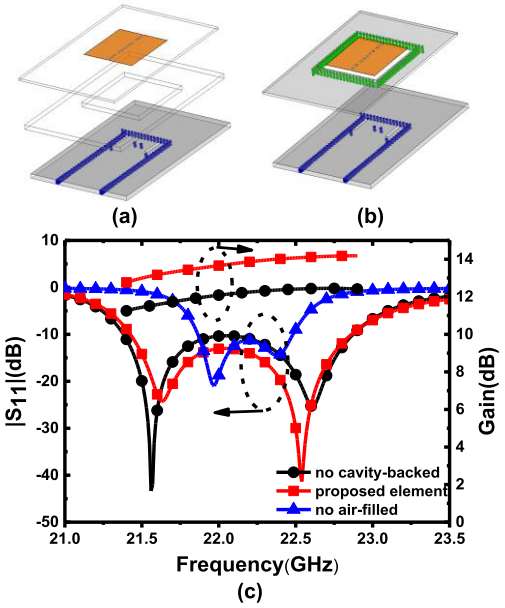

FIGURE 7. (a) Patch radiator without backed cavity, (b) patch radiator without filled air, (c) simulated S-parameter and gain curve of the element with different structures.

bandwidth can be enhanced by increasing the substrate thickness. Though the surface wave will be strengthened, the SIW cavity back structure can solve this problem effectively. Two other structures are considered and compared to verify the above analysis, which is shown in Fig.7 (a) and (b). The first one is the structure without backed cavity, while the second one is the structure without filled air. Minor changes have been made for the dimensions of the second type to achieve better impedance matching. As shown in Fig.7 (c), the air-filled structure can be used to decrease the quality factor and broaden the impedance bandwidth, while the cavity-backed structure can suppress the surface wave and enhance the gain property.

C. PARAMETRIC STUDY

The antenna element is designed with three F4B layers ($\varepsilon_r = 2.2, \tan\delta = 0.0007$) and optimized with the full wave simulation software-Ansoft HFSS. The parameters of the element are listed in Table 1.

The reflection coefficient and radiation performance are simulated and optimized to future explore the working principle. Major parameters such as slot length of patch (*Ls*2), slot length of SIW (*Sl*), the positions of the matching pins and coupling slots (*Px, Py, Dx*) as well as geometry of the cavity-backed structure are investigated. The simulated reflection coefficients with different parameters are shown in Fig. 8 (a)-(f). A new resonant point is introduced by the loading pins. Consequently two resonant points are observed. Furthermore, several additional design freedoms are achieved for better impedance matching. Fig. 8 (a) and (b) indicate that the first resonant frequency is hardly affected by the radiating patch and the second pair of matching pins, while the second

TABLE 1. Parameters for the proposed antenna element.

Symbol	Value	Symbol	Value	Symbol	Value
W(mm)	12	$Ls1$(mm)	4.7	$Ls2$(mm)	2.5
Sl(mm)	5	Sw(mm)	0.7	Dx(mm)	3.6
$Wcav$(mm)	15.4	$Px1$(mm)	4.7	$Px2$(mm)	0.8
W_{TE20}(mm)	11	h_1(mm)	0.5	h_2/h_3(mm)	1

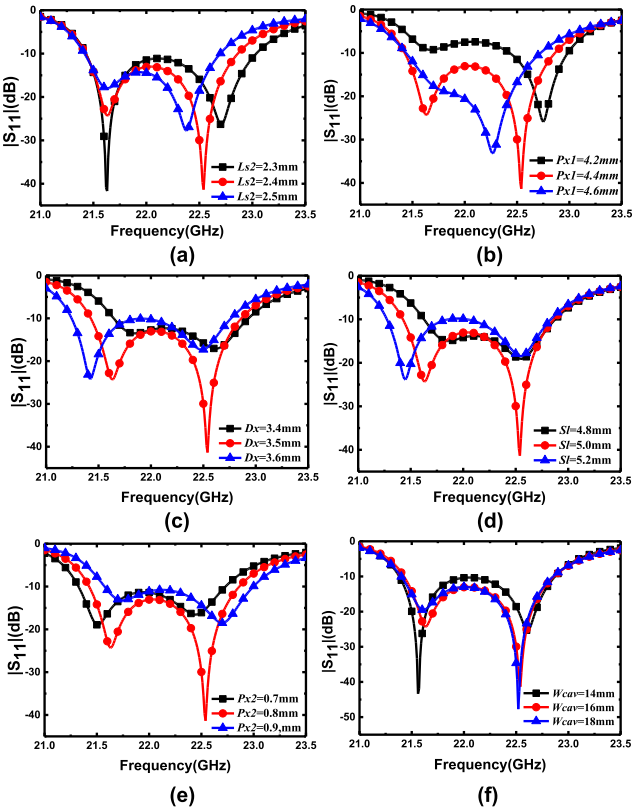

FIGURE 8. Simulated S-parameter of the element with different parameters. (a) *Ls*2, (b) *Px*1, (c) *Dx*, (d)*Sl*, (e) *Px*2, (f) *Wcav*.

resonant frequency is affected dramatically. As the length of slots increases, the second resonant frequency decreases because of the extended current path. As shown in Fig. 8 (c) and (d), the first resonant frequency is mainly affected by the position and the length of the coupling slots. While the position of the first pair of matching pins influences both resonant frequency and the impedance matching, which is shown in Fig. 8 (d). Fig. 8 (f) illustrates that the size of SIW cavity has little effect on the reflection coefficient. However, the cavity backed structure can be used to suppress the surface wave to improve the element gain and the isolation in array application as mentioned above.

D. SIMULATED RESULTS OF THE ANTENNA ELEMENT

The simulated gain and $|S_{11}|$ of the antenna element are given in Fig. 7 (c). The -10 dB impedance bandwidth is 6.9%. The peak gain reaches up to 14.2dBi at 22.7GHz, and the gain is higher than 13.5 dBi over the whole impedance bandwidth. The radiation patterns of 22.7GHz are shown

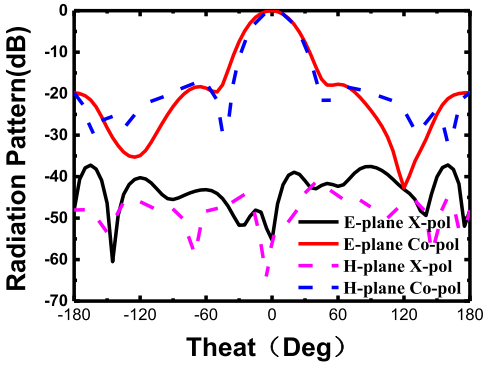

FIGURE 9. Simulated radiation patterns of antenna element at 22.7GHz.

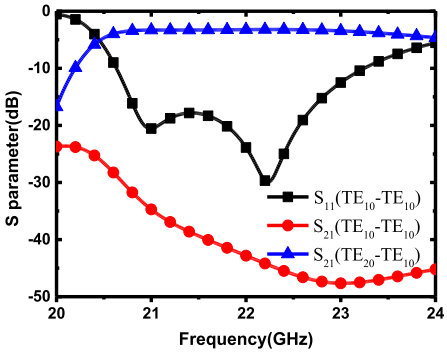

FIGURE 11. The S-parameters of the mode transducer based on two layer substrates.

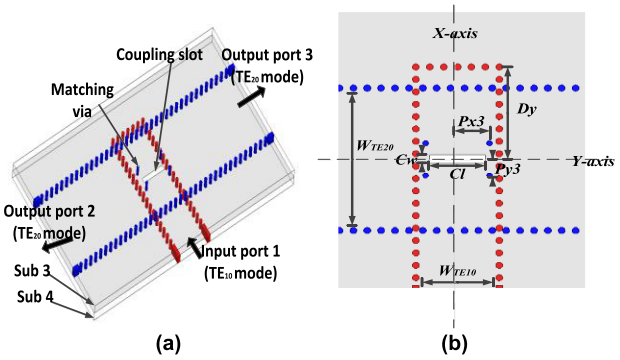

FIGURE 10. The geometry of the mode transducer based on two substrate layers. (a) 3D view, (b) top view. ($W_{TE10} = 7$mm, $W_{TE20} = 11$mm, $Px3 = 2.3$mm, $Py3 = 1.3$mm, $Cl = 4$mm, $Cw = 0.7$mm, $Dy = 7.2$mm).

in Fig.9. The beamwidths of both E-plane and H-plane are so narrow that the pattern of the element factor will not cover the grating lobes of the array factor. Thus high sidelobe level in the electrically large array could be avoided. Furthermore, the cross-polarization levels of the element are lower than −30 dB in both E-plane and H-plane.

III. 2 × 2 ARRAY WITH DIFFERENTIAL FEED TECHNOLOGY

A 2 × 2 electrically large air-cavity-backed patch antenna array with differential feeding network is proposed in this section. The differential feeding network consists of an anti-phase power divider based on a TE_{20}-mode SIW structure and two TE_{10}-TE_{20} mode transducers. All the structures are based on the substrate of F4B ($\varepsilon_r = 2.2$, $\tan\delta = 0.0007$) with thickness of 1mm. The geometries and working principle of the structures are described as follows.

A. TE_{10}-TE_{20} MODE SIW TRANSDUCER BASED ON DOUBLE SUBSTRATE LAYERS

As mentioned above, the ELA element resonant on TM_{30} mode is fed by TE_{20}-mode SIW. A mode transducer is adopted to excite the TE_{20} mode without TE_{10} mode, which is combined with a 3dB power divider to achieve the array of elements in H-plane. Fig. 10 shows the geometry of the mode transition structure, which consists of two substrate layers. The TE_{20}-mode SIW in the upper layer can be excited by the TE_{10}-mode SIW in the lower layer. The power of TE_{10} mode is equally divided into port 2 and 3 through the coupling slot. The metallic pins with the radius of 0.25mm are adopted to achieve impedance matching. Fig. 11 shows the simulated impedance bandwidth is from 20.5 GHz to 23.5 GHz, covering the bandwidth of antenna element. The S_{21} of TE_{10}-TE_{10} is lower than −30dB, which means that almost all the energy of TE_{10} is converted into TE_{20} mode. The simulated loss of the structure is 0.4 dB.

B. ANTI-PHASE POWER DIVIDER BASED ON TE_{20}-MODE SIW

Fig. 12 (a) shows the electric field distribution of the power divider. As indicated, the electric field distribution of the TE_{20} mode is asymmetrical. The antenna elements are fed by the TE_{20}-mode SIW, so the differential feeding technology is required in E-plane of the array. Just using the asymmetrical phase distribution of TE_{20} mode, the anti- phase power divider based on TE_{20}-mode SIW can be formed with only one substrate layer. The geometry of the power divider is shown in Fig.12 (b). Several metallic pins with radius of 0.25mm are introduced to achieve good impedance matching. The simulated reflection coefficients and the phase difference between output ports of the power divider are shown in Fig. 13. Good amplitude and phase performances are achieved over the bandwidth of the antenna element. And the simulated loss is 0.3 dB.

C. TE_{10}-TE_{20} MODE SIW TRANSDUCER BASED ON SINGLE LAYER

In order to excite the anti-phase power divider with TE_{20} mode, another new mode transducer based on SIW structure is designed. Only one layer is used for the sake of simplification [18]. The geometry and the electric field distribution are illustrated in Fig. 14. Four matching pins with radius of 0.25mm are optimized at the position of structural corner to achieve good impedance matching and conversion efficiency. The simulated S-parameters of the single layer transducer are

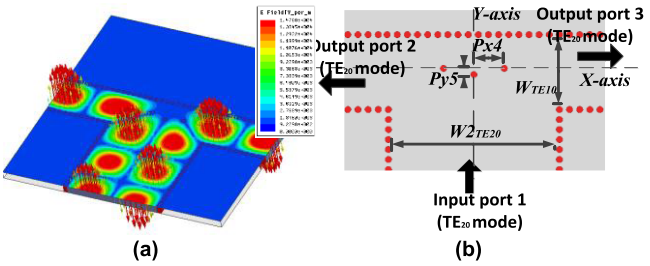

FIGURE 12. (a) The electric field distribution of the anti-phase power divider, (b) the geometry of the anti-phase power divider. ($W2_{TE20} = 13$mm, $Px4 = 0.3$mm, $Py5 = 0.2$mm).

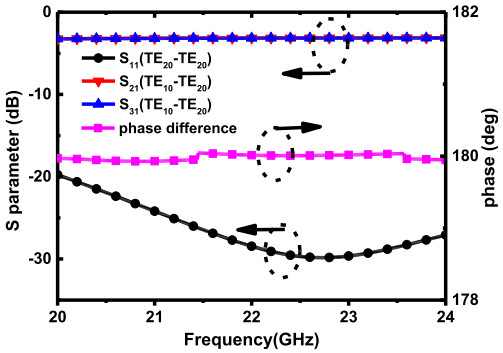

FIGURE 13. The simulated S-parameter and phase difference between output ports of the anti-phase power divider.

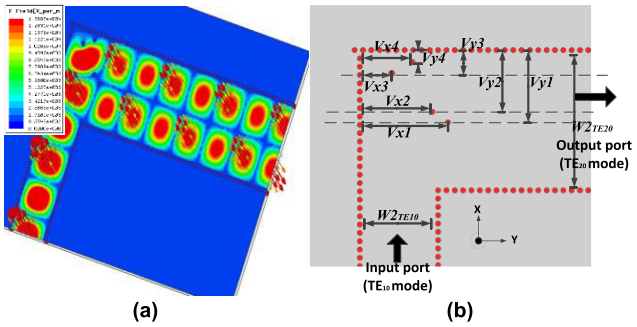

FIGURE 14. (a) The electric field distribution of the single-layer mode transducer, (b) the geometry of the single-layer mode transducer. ($W2_{TE10} = 7$mm, $Vx1 = 4.1$mm, $Vx2 = 6.7$mm, $Vx3 = 2.8$mm, $Vx4 = 4.8$mm, $Vy1 = 6.7$mm, $Vy2 = 5.7$mm, $Vy3 = 2$mm, $Vy4 = 0.9$mm).

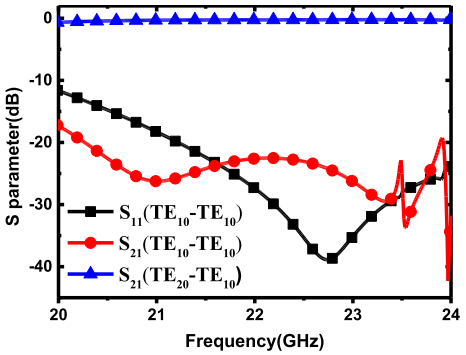

FIGURE 15. The S-parameters of the single-layer mode transducer.

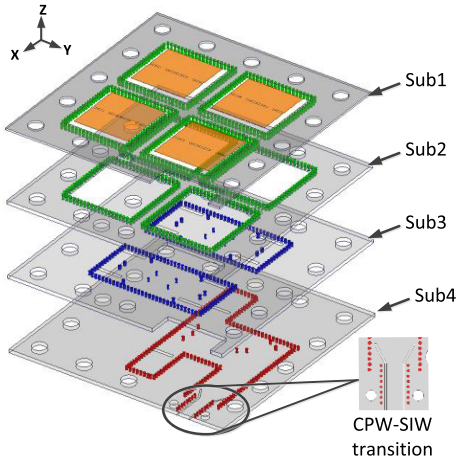

FIGURE 16. The geometry of the proposed 2 × 2 antenna array with differential feeding network.

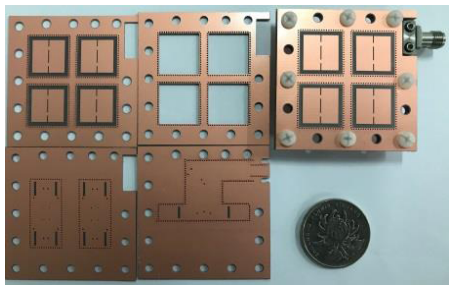

FIGURE 17. Photograph of the fabricated antenna array.

shown in Fig. 15. And the S_{21} of TE_{10}-TE_{10} is lower than −20dB, which means the good conversion efficiency.

D. COMPLETE STRUCTURE OF THE 2 × 2 ANTENNA ARRAY

The complete structure of the 2 × 2 antenna array is designed by using the differential feeding network above. The geometry of the array is shown in Fig.16. The whole structure consists of four substrates, which can be fabricated by conventional sing-layer PCB technology. The radiating patches are printed on the top surface of Sub.1. The air-filled cavities are introduced in Sub.2. Thus the cavity-backed structures are realized in Sub.1 and Sub.2, while Sub.3 contains the TE_{20}-mode SIW feeding structure. Sub.4 contains two mode transducers and an anti-phase power divider. In addition, the CPW-SIW structure is introduced in Sub.4 to feed the antenna array [19]. The processes of the signal transmission can be summarized as follows.

(1) The energy is fed into the SIW by the CPW-to-SIW transition structure. The TE_{10}-mode signal in the SIW propagates through the first mode transducer.

(2) The TE_{20}-mode signal of the anti-phase power divider is excited through the first mode transducer.

(3) The energy of TE_{20}-mode signal in the SIW power divider is equally divided into TE_{10}-mode with opposite phase to achieve the differential feeding.

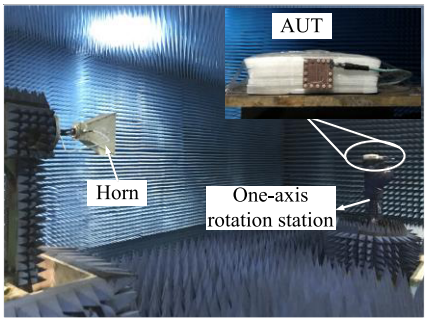

FIGURE 18. Photograph of the test equipment.

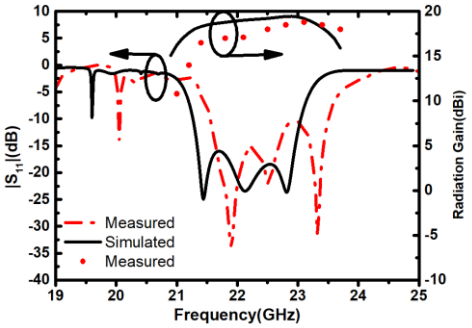

FIGURE 19. Comparison of the simulated and measured bandwidths and gains of the proposed 2 × 2 antenna array.

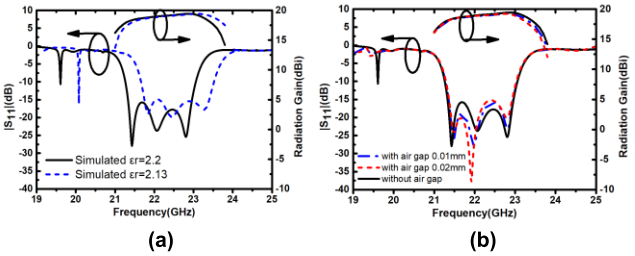

FIGURE 20. Simulated $|S_{11}|$ and gain of the array with different dielectric constant and thicknesses of the air gap. (a) different dielectric constant, (b) different thickness of the air gap.

(4) The TE_{10}-mode signal in the output port of anti-phase power divider propagates through the second mode transducer and excites the TE_{20}-mode signal in the Sub.3, which feeds the antenna elements.

(5) Finally, the TE_{20}-mode SIW feeding structures are excited to feed the antenna elements resonant on TM_{30} mode.

And the design procedure can be summarized as follows.

(1) Design the patch which resonant on TM_{30} mode, and adjust the slot length $Ls1$ and $Ls2$ to make sure the element has the maximum directivity.

(2) Design the TE_{20} mode SIW feeding structure. Tune the dimensions and positions of the coupling slots and matching pins to achieve a good matching at the maximum directivity point.

(3) Design the double layer mode transducer, anti-phase power divider and single layer mode transducer respectively. Adjust the physical dimensions to achieve good transmission efficiency and mode conversion efficiency.

(4) The above structures are spliced together to complete the design of feeding network and antenna array.

(5) Finally, design the CPW-SIW transition structure to make sure the probe can be used to feed the antenna array.

IV. EXPERIMENTAL RESULTS OF THE ANTENNA ARRAY

A prototype of the designed antenna array was fabricated and measured for verification. The photograph of the four PCB substrates and the whole antenna array structure is exhibited in Fig. 17. The array is fabricated by using the conventional low-cost single layered PCB process. The four layers are fabricated individually and then assembled together by plastic screws. The ET-launch SMA probe-to-coaxial adaptor is adopted for measurement. The S-parameters of the proposed antenna were measured by an Agilent N5230A network analyzer, and the radiation characteristics were measured by an in-house far-field microwave antenna measurement system. The photograph of test equipment is shown in Fig.18.

A. IMPEDANCE BANDWIDTH AND RADIATION GAIN

The simulated and measured $|S_{11}|$ of the fabricated antenna array are shown in Fig.19. Acceptable agreement between the simulation and measurement can be observed. The simulated bandwidth is 8.3% (21.23 to 23.05 GHz), and the measured bandwidth is 9% (21.5 to 23.5 GHz), which is slightly shifted to high frequency. In order to analyze the cause of deviation, we simulated the array with different dielectric constant and thicknesses of the air gap. According to the experience, the dielectric constant of PCB laminates will have some small change at high frequency, and as the frequency increases, the dielectric constant decreases slightly which will affect the antenna performances. As shown in Fig.20 (a), when the dielectric constant of the substrate was set as 2.13, the simulation results were shifted towards high frequency and basically consistent with the measured results. Since the substrates are assembled together by plastic screws, the effect of air gaps between substrates should be considered. The simulated results of the array with different thicknesses of the air gaps are given in Fig. 20 (b). It can be seen that the air gap mainly affects the matching results, but not the resonant frequency point. And the gains have a slight decrease in the high frequency part. Base on the above analyses, the discrepancy is mainly generated by the change of dielectric constant. The simulated and measured gain curves are also illustrated in Fig. 19. The method of finding the gain is using the comparison method. The gain of the antenna can be expressed as

$$G = Gs + Px - Ps \tag{6}$$

where G is the gain of the antenna under test, and Gs is the gain of standard antenna. While the Px and Ps are received power of the tested antenna and standard antenna respectively. The simulated gains are above 18.5 dBi in the operating

TABLE 2. Comparison between proposed antenna and reported typical antenna array.

Ref	Freq (GHz)	Feeding network	Type	No.of Elements	Impedance Bandwidth	Max Gain(dBi)	X-pol Level(dB)	Aperture Efficiency
[12]	28	TE_{20}-mode SIW (Series-parallel)	SIW-based patch antenna	16	8.5%	19.1	-25	48.2%
[13]	38	TE_{10}-mode SIW (Series-parallel)	cavity-backed patch antenna	16	8.7%	18	-21	24.1%
[14]	60	Stripline (parallel)	L-probe patch with Soft Surface	16	29%	17.5	-20	75%
[15]	60	TE_{10}-mode SIW (parallel)	Cavity-backed wide slot antenna	8	11.6%	12.2	-25	n.a.
[16]	14	GWG (parallel)	Slot antenna with GWG	4	21%	12.2	-24	75%
Our work	**22**	**TE_{20}-mode SIW (parallel)**	**Cavity-backed patch antenna based high-order mode**	**4**	**9%**	**18.9**	**-30**	**90%**

band, and the peak gain reaches up to 19.4 dBi at 22.8 GHz, which are achieved by only four elements. The measured 3dB gain bandwidth covers the impedance bandwidth. The measured peak gain is 18.9 dBi at 23.2 GHz. The measured aperture efficiency is 90% according to the formula (7), where the λ, G, and A_p are the wavelength in free space, measured antenna gain, and aperture area of antenna, respectively. The aperture of the antenna is a square area with the side length of 34mm, which covering the four radiation cavities.

$$\varepsilon_{ap} = \frac{G\lambda^2}{4\pi A_p} \tag{7}$$

B. RADIATION PATTERNS

The simulated and measured radiation patterns of the 2×2 antenna array at 21.6 GHz, 22.2 GHz and 22.8 GHz are given in Fig. 21. The results are in good agreement in both H-planes and E-planes. Good broadside radiation patterns are realized. Since the element gain value is considerable, the sidelobe levels of the array are not very high, which is much better than that in [12]. Thanks to the TE_{20}-mode SIW and differential feeding structure, the cross-polarization level is very low, which is below -30dB in both E-planes and H-planes.

C. COMPARISON

The performance comparisons between our work and other designs are listed in Table 2. As indicated, at least 16 elements are needed to obtain high gain of over 17 dBi in the former designs [12]–[14]. However, better performances can be achieved by only 4 elements in our design. The high gain value of the antenna array is owing to the ELP element which resonant on TM_{30} mode. Due to the ELP of the element, the antenna element has a larger radiation aperture to enhance the gain. And the slots on the surface of the patch provide a new radiation source and maintain the field distribution more uniform to enhance the aperture efficiency. Additionally, the cavity-backed structure can be used to suppress the surface wave, which can enhance the gain further. Symmetrical radiation patterns and low cross-polarization levels are achieved

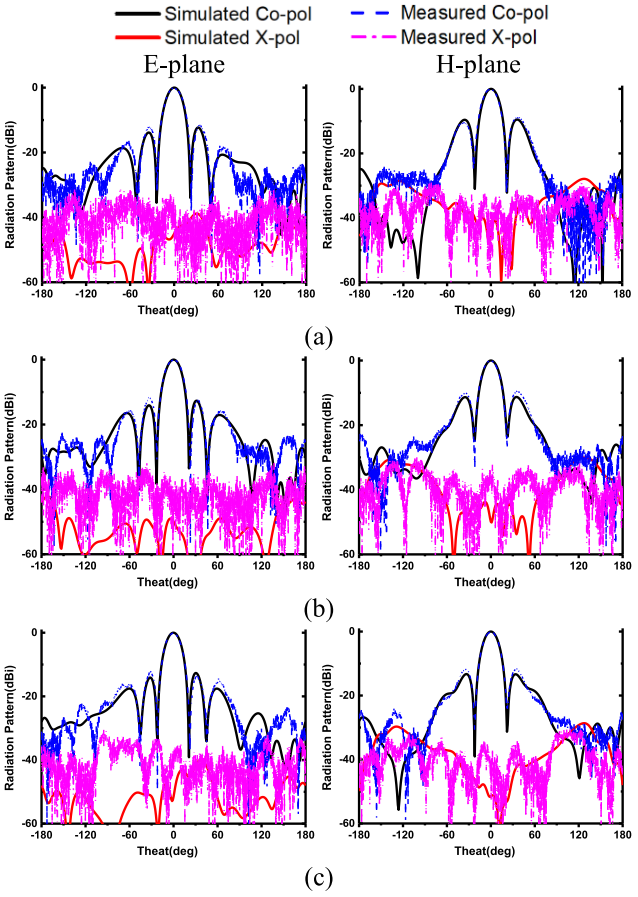

FIGURE 21. Measured and simulated radiation patterns of the proposed antenna array. (a) 21.6GHz, (b) 22.2GHz, (c) 22.8GHz.

because of the symmetrical physical structure and the differential feeding network.

Due to the high gain property of the antenna element with ELP, fewer elements are needed for array design while maintaining the same gain level. Furthermore, the feeding structure of the electrically large array based on high-order mode can be more compact. Thus higher aperture efficiency can be achieved which reaches up to 90%. What should be

mentioned is that the impedance bandwidth is in intermediate level compared with the other designs. It attributes to the high quality factor caused by strong resonance of high-order mode.

V. CONCLUSION

In this paper, a TE_{20}-mode SIW feed air-cavity-backed patch antenna element resonant on TM_{30} mode with ELP was firstly designed to improve machining tolerance. High gain of 14.2dBi was achieved for the electrically large element. Then one 2×2 array with differential feeding network was designed and fabricated for verification. The antenna array has high gain value of 18.9 dBi with only four elements, which enhances the aperture and radiation efficiency. Additionally, the array overcomes the problem of severe side lobe caused by ELA. The array has good radiation performances, such as symmetrical radiation patterns and low cross-polarization levels. The proposed antenna array with ELP has potential application in the MMW band communication systems in future.

REFERENCES

[1] Y.-M. Pan, K. W. Leung, and K.-M. Luk, "Design of the millimeter-wave rectangular dielectric resonator antenna using a higher-order mode," *IEEE Trans. Antennas Propag.*, vol. 59, no. 8, pp. 2780–2787, Aug. 2011.

[2] G.-H. Zhang, Y.-Q. Fu, C. Zhu, D.-B. Yan, and N.-C. Yuan, "A circular waveguide antenna using high-impedance ground plane," *IEEE Antennas Wireless Propag. Lett.*, vol. 2, no. 1, pp. 86–88, 2003.

[3] Y. Zhao, Z. Zhang, and Z. Feng, "An electrically large metallic cavity antenna with circular polarization for satellite applications," *IEEE Antennas Wireless Propag. Lett.*, vol. 10, pp. 1461–1464, 2011.

[4] Y. Zhao, Z. Zhang, and Z. Feng, "An electrically large circularly polarized metallic cavity antenna with wide beamwidth for satellite applications," in *Proc. ICMMT*, Shenzhen, China, May 2012, pp. 1–4.

[5] W.-Q. Cao, W. Hong, and Y. Cai, "Microstrip-line-slot fed EDPA elements and array with ELP," *IET Microw. Antennas Propag.*, vol. 10, no. 12, pp. 1304–1311, 2016.

[6] Y. Cai, Z. Q. Qian, W. Q. Cao, Y. S. Zhang, and L. Yang, "Electrically large resonant cavity loaded with ε-negative and μ-negative metamaterials," *IEEE Antennas Wireless Propag. Lett.*, vol. 15, pp. 294–297, 2016.

[7] W. Cao, B. Zhang, J. Jin, W. Zhong, and W. Hong, "Microstrip antenna with electrically large property based on metamaterial inclusions," *IEEE Trans. Antennas Propag.*, vol. 65, no. 6, pp. 2899–2905, Apr. 2017.

[8] P. Juyal and L. Shafai, "A novel high-gain printed antenna configuration based on TM_{12} mode of circular disc," *IEEE Trans. Antennas Propag.*, vol. 64, no. 2, pp. 790–796, Feb. 2016.

[9] P. Juyal and L. Shafai, "A high-gain single-feed dual-mode microstrip disc radiator," *IEEE Trans. Antennas Propag.*, vol. 64, no. 6, pp. 2115–2126, Jun. 2016.

[10] P. Juyal and L. Shafai, "Sidelobe reduction of TM_{12} mode of circular patch via nonresonant narrow slot," *IEEE Trans. Antennas Propag.*, vol. 64, no. 8, pp. 3361–3369, Aug. 2016.

[11] X. Zhang, L. Zhu, and Q.-S. Wu, "Sidelobe-reduced and gain-enhanced square patch antennas with adjustable beamwidth under TM_{03} mode operation," *IEEE Trans. Antennas Propag.*, vol. 66, no. 4, pp. 1704–1713, Apr. 2018.

[12] H. Jin, W. Che, K. Chin, W. Yang, and Q. Xue, "Millimeter-wave TE_{20}-mode SIW dual-slot-fed patch antenna array with a compact differential feeding network," *IEEE Trans. Antennas Progag.*, vol. 66, no. 1, pp. 456–461, Jan. 2017.

[13] T. Y. Yang, W. Hong, and Y. Zhang, "Wideband millimeter-wave substrate integrated waveguide cavity-backed rectangular patch antenna," *IEEE Antennas Wireless Propag. Lett.*, vol. 13, pp. 205–208, 2014.

[14] L. Wang, Y. X. Guo, and W. X. Sheng, "Wideband high-gain 60-GHz LTCC L-probe patch antenna array with a soft surface," *IEEE Trans. Antennas Propag.*, vol. 61, no. 4, pp. 1802–1809, Apr. 2013.

[15] K. Gong, Z. N. Chen, X. Qing, P. Chen, and W. Hong, "Substrate integrated waveguide cavity-backed wide slot antenna for 60-GHz Bands," *IEEE Trans. Antennas Propag.*, vol. 60, no. 12, pp. 6023–6026, Dec. 2012.

[16] A. U. Zaman and P.-S. Kildal, "Wide-band slot antenna arrays with single-layer corporate-feed network in ridge gap waveguide technology," *IEEE Trans. Antennas Propag.*, vol. 62, no. 6, pp. 2992–3001, Jun. 2014.

[17] C. A. Balanis, *Antenna Theory: Analysis and Design*. Hoboken, NJ, USA: Wiley, 2005.

[18] S. Matsumoto, I. Ohta, K. Fukada, T. Kawai, K. Iio, and T. Kashiwa, "A TE_{10}-TE_{20} mode transducer utilizing a right-angled corner and its application to a compact H-plane out-of-phase power divider," in *Proc. Asia–Pacific Microw. Conf.*, Dec. 2009, pp. 1008–1011.

[19] X.-P. Chen and K. Wu, "Low-loss ultra-wideband transition between conductor-backed coplanar waveguide and substrate integrated waveguide," in *IEEE MTT-S Int. Microw. Symp. Dig.*, Boston, MA, USA, Jun. 2009, pp. 349–352.

WENFANG PENG was born in Fuxin, Liaoning, China, in 1993. He received the B.S. degree in electromagnetic field and wireless technology from Xidian University, Xi'an, China, in 2016, and the M.S. degree in electronic science and technology from the Army Engineering University of PLA, Nanjing, China, in 2018. His current research interests include millimeter-wave antennas, antenna array technology, metamaterials, and their applications to microwave components and antennas.

WENQUAN CAO received the B.S. and Ph.D. degrees from the Institute of Communications Engineering, Nanjing, China, in 2008 and 2014, respectively. He is currently a Lecturer with the Institute of Communications Engineering. He has authored and co-authored more than 100conference and journal papers, including more than 20 in IEEE periodicals. His current research interests include microstrip antennas, metamaterials, and their applications to microwave components and antennas. He is currently serving as a Reviewer for the IEEE Microwave and Wireless Components Letters and the IEEE Antennas and Wireless Propagation Letter.

ZUPING QIAN was born in Haimen, Jiangsu, China, in 1961. He received the B.S. and M.S. degrees in applied mathematics from Hunan University, Changsha, China, in 1982 and 1985, respectively, and the Ph.D. degree in microwave techniques from Southeast University, Nanjing, China, in 2000. From 1985 to 1999, he was with the Institute of Communications Engineering, Nanjing, China, as a Lecturer and later as an Associate Professor. Since 2000, he has been a Professor with the College of Communications Engineering, PLA University of Science and Technology, Nanjing, China. He authored several books such as *Electromagnetic Compatibility*, *Antenna*, and *Propagation*. He has authored over 80 international and regional refereed journal papers. His research interests include antenna, metamaterials, computational electromagnetics, array signal processing, and EMI/EMC.